# Ambient Noise and Earthquake Surface Wave Phase Velocity Tomography of the South American Lithosphere


Lúcio Quadros[1], Amr El-Sharkawy[2, 3], Marcelo Assumpção[1], Sergei Levedev[4] and Thomas Meier[2]

[1]*Institute of Astronomy, Geophysics and Atmospheric Sciences, University of São Paulo, 05508-090, São Paulo, Brazil*

[2]*Institute of Geoscience, Christian-Albrechts University, 24118, Kiel, Germany*

[3]*National Research Institute of Astronomy and Geophysics (NRIAG), 11421, Helwan, Cairo, Egypt*

[4]*Department of Earth Sciences, University of Cambridge, Cambridge, United Kingdom*


## Introduction

There are several important open questions regarding the characteristics and tectonic evolution of the South American Lithosphere. The development of new automated techniques to measure earthquake-based interstation phase velocities allows for more detailed imaging of the lithosphere. For this presentation, we calculated Rayleigh-wave phase velocities using the earthquake records from 1,022 broadband seismic stations (South America, Antarctica and the Caribbean) operated between 1990 and 2020 for periods between 5 and 200 s. We plan to include ambient noise data to better constrain the crustal structure.

## Methodology

### 1) Phase velocity extraction

The two-station method is a way to measure surface-wave group and phase velocities using earthquakes closely aligned with a pair of stations. We did that by cross-correlating the earthquake records for pairs of stations. We used the cross-correlation because it has the advantage of being less affected by uncorrelated noise and the contribution of the fundamental mode is enhanced by the product of the amplitude spectra.
Here is an example from Soomro et al., 2016:

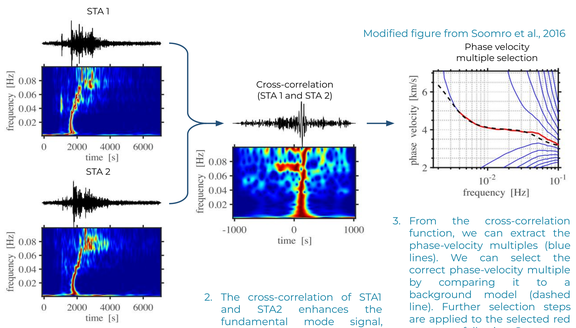


1. Here are the records of an event for the stations STA1 and STA2. The time-frequency representation of each signal is shown below. The red color marks the Rayleigh wave fundamental mode and becomes poorly defined for frequencies above 0.06 Hz.
2. The cross-correlation of STA1 and STA2 enhances the fundamental mode signal, even for frequencies above 0.06 Hz.
3. From the cross-correlation function, we can extract the phase-velocity multiples (blue lines). We can select the correct phase-velocity multiple by comparing it to a background model (dashed line). Further selection steps are applied to the selected red segment, following Soomro et al., 2016: (1) fit between the background model and phase-velocity multiple; (2) curve smoothness; (3) curve length.

### 2) Averaging phase velocities for each interstation path

Averaging example for two stations in Europe.

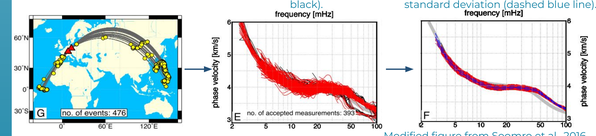


Because the phase-velocity curves calculated for each pair of stations can have some variability, especially for different propagation directions, we apply some further quality control before taking the final average. The following implementation is based on Soomro et al., (2016):

1. outlier rejection (15% of the outermost data);
2. a minimum of 5 measurements for each frequency;
3. for each direction: the mean phase-velocity curve and standard deviation (std1 and std2) must be within $1th_{std} = 5 \times max(std1, std2)$
4. The standard deviation of all measurements should be lower than 3%;
5. Curve length is checked again;

## Methodology cont.

### 3) Phase velocity maps

We conducted a simultaneous isotropic and anisotropic phase-velocity inversion for Rayleigh waves following the work of Deschamps et al. (2008). We accounted for the 2ψ and 4ψ contributions for the anisotropic part (Smith and Dahlen, 1973). The contributions to the phase velocity anomaly for a latitude θ and longitude φ are described by Deschamps et al. (2008):

$$\delta C(\varphi,\theta) = \delta C_{iso}(\varphi,\theta) + \delta C_{2\psi}(\varphi,\theta) + \delta C_{4\psi}(\varphi,\theta)$$

where δCiso(φ, θ) is the isotropic anomaly and δC2ψ(φ, θ) and δC4ψ(φ, θ) are the 2ψ and 4ψ anisotropic anomalies that are defined as

$$\delta C_{2\psi}(\varphi,\theta) = A_{2\psi}cos(2\psi) + B_{2\psi}sin(2\psi)$$

and

$$\delta C_{4\psi}(\varphi,\theta) = A_{4\psi}cos(4\psi) + B_{4\psi}sin(4\psi)$$

where ψ is the local ray azimuth. The four anisotropic coefficients are defined for each latitude and longitude as A2ψ, B2ψ, A4ψ and B4ψ.
The amplitudes of anisotropic anomalies and direction of fast propagation are defined as, respectively:

$$\begin{cases} \Lambda_{2\psi} = \sqrt{A_{2\psi}^2 + B_{2\psi}^2} \\ \Lambda_{4\psi} = \sqrt{A_{4\psi}^2 + B_{4\psi}^2} \end{cases} \quad \text{and} \quad \begin{cases} \Theta_{2\psi} = \frac{1}{2} arctan\left(\frac{B_{2\psi}}{A_{2\psi}}\right) \\ \Theta_{4\psi} = \frac{1}{4} arctan\left(\frac{B_{4\psi}}{A_{4\psi}}\right) \end{cases}$$

### 4) Depth inversion

In other to interpret the phase velocities in terms of shear wave velocities as a function of depth we applied an inversion algorithm based on the particle-swarm-optimization technique. As described in Wilken and Rabbel (2012), the objectives of the implementation of the PSO are to:

1. reduce dependence with a priori information related to an initial model;
2. avoid the computation of gradients that can cause numerical instabilities;
3. thoroughly explore the parameter space to enhance the likelihood of finding a proper solution;
4. allowing niche solutions to exist, as it is expected for a non-unique inverse problem.

The basis of the model described by Wilken and Rabbel (2012) each particle moves in the parameter space based on three components of motion described by the displacement vector vij(t + 1) below:

$$v_{ij}(t+1) = \underset{\downarrow\ I}{\omega v_{ij}(t)} + \underset{\downarrow\ II}{c_1 r_{1j}(y_{Cij}(t) - x_{ij}(t))} + \underset{\downarrow\ III}{c_2 r_2 (y_{Gj}(t) - x_{ij}(t))}$$

where xij (t) and vij (t) are the position and displacement of a particle i in the parameter space j for an iteration t. The weighting factors c1, c2 and ω control the exploration and convergence of the swarm. The r1j and r2j are random numbers between 0 and 1 distributed uniformly.
**Term I:** moment from previous iteration;
**Term II:** component in the direction of the best position for a particle;
**Term III:** component in the direction of the best position for all particles.
The model convergence is speeded up through local random search after each iteration.

## Data

### Data selection

Raypath coverage and number of events per path

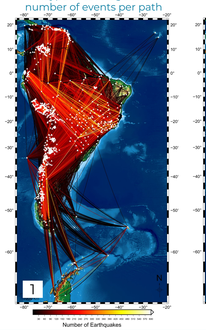


Number of events per station

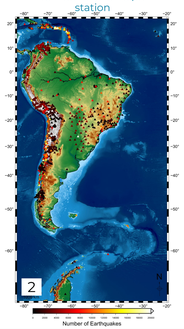


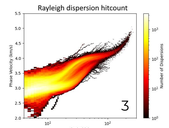


We calculated Rayleigh and Love-wave phase velocities using earthquake records from 1,022 stations (South America, Antarctica and the Caribbean) between 1990 and 2020. A total of 1,069,259 earthquakes were selected based on four following criteria:

## Data cont.

1. events aligned within 10° of the great circle path between a pair of stations;
2. a linearly increasing minimum magnitude between 4 and 6 Mw as a function of the epicentral distance;
3. maximum magnitude of 8 Mw;
4. epicentral distances between 2.5° and 30°.

Following this process, we obtained 30,726 broad-band dispersion measurements between 4 and 315s for Rayleigh waves.

This Fig. 1 shows that our ray path covers most of South America, having a higher number of crossings inside Brazil. The stations in the Caribbean, Andes and some of the permanent Brazilian seismographic stations provide most of the earthquake records (fig. 2).

Fig. 3 shows a hit count plot for all the dispersion curves for both Rayleigh and Love waves. We can see that most of our Rayleigh curves are below 100 s.

## Results

### Phase velocity maps

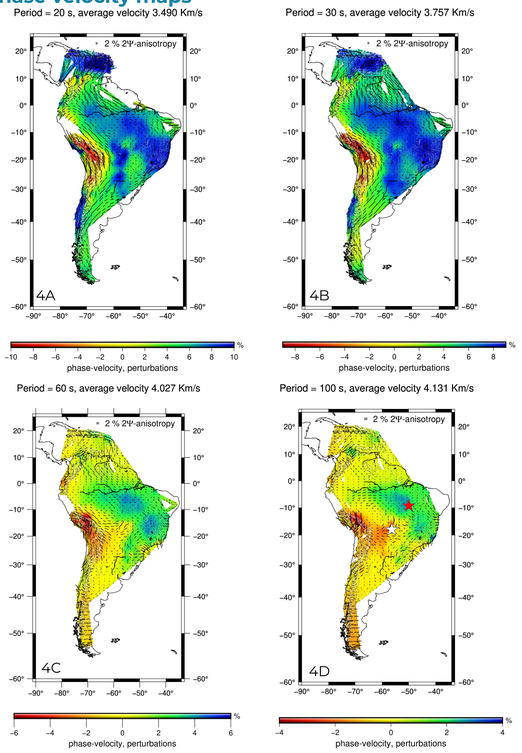


## Results cont.

Fig. 4 shows Rayleigh phase-velocity maps for the periods of 20-, 30-, 60- and 100 s. The velocity perturbations are plotted in relation to a regional average (top of each figure) and the fast direction of the anisotropy is plotted as the black bar.

Some observations for 20 and 30 s:

1. Pronounced high velocities (>6%) associated with the cratonic areas inside Brazil and to the north in the Caribbean oceanic plate;
2. Lower velocities (~4%) inside the cratonic areas associated with sedimentary basins, such as Paraná, Parecis and Parnaíba basins. As expected we observe strong lower velocities below the Altiplano Boliviano region associated with the deep Andean range roots;
3. strong NW-SE anisotropy north of the Amazonian river.

For 60 and 100 s:

1. The high velocities (~3%) in the eastern portion of Brazil are correlated to the deep roots of the oldest region of the Amazonian craton and the São Francisco craton.
2. Lower velocities (~-2%) can be seen below the Pantanal basin area and are well correlated with the lower depths of the Lithosphere-Asthenosphere Boundary using an Adjoint Waveform Tomography by Ciardelli et al. (2022). The anisotropy below this region shows a preliminary direction of NE-SW and it is well correlated with the results found by Melo et al. (2018) using shear wave splitting.11

### Depth inversion

We show an isotropic Rayleigh-wave dispersion curve inversion for a node very close to the Pantanal basin (white star) characterized by thin crust and thin lithosphere and another node in the Amazonian craton (red star) characterized by thick lithosphere. Those results are shown after about 10,000 forward calculations and were based on perturbations of a background model (CRUST1.0 + PREM) following **step 4**. We inverted for velocities and discontinuity depths.

Fig. 5A/6A show the accepted models as a red line (weighted average of all models inside the dashed red lines) and the best model as black. Fig. 5B/6B show the fit between the observed dispersion curve (black), its uncertainty (dashed black) and synthetic (red). Fig. 5C/6C is similar to A, but it shows some of the best-fitting models from best (blue) to worst (red). Quadratic perturbations were applied to the crust (blue line, 5/6D), cubic to the mantle (red line, 5/6D) and linear below the transition zone, 430 km (green line, 5/6D). The circles and dashes show the layers and discontinuities included in the inversion.

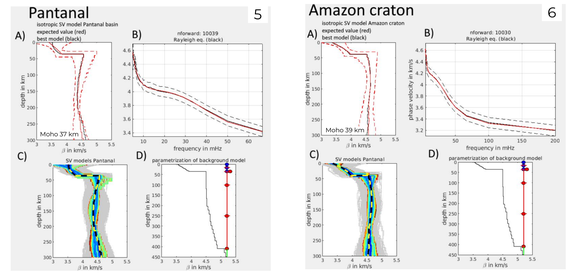


## Acknowledgements


This Ph.D. project was funded by the Coordenação de Aperfeiçoamento de Pessoal de Nível Superior (CAPES) and Programa de Doutorado-sanduíche no Exterior by CAPES. This research was supported in part through high-performance computing resources available at the Kiel University Computing Centre.


References

Get the abstract